



HAL
open science

Phase diagram of the Anderson transition with atomic matter waves

Matthias Lopez, Jean-François Clément, Gabriel Lemarié, Dominique Delande, Pascal Szriftgiser, Jean Claude Garreau

► **To cite this version:**

Matthias Lopez, Jean-François Clément, Gabriel Lemarié, Dominique Delande, Pascal Szriftgiser, et al.. Phase diagram of the Anderson transition with atomic matter waves. *New Journal of Physics*, 2013, 15, pp.065013. 10.1088/1367-2630/15/6/065013 . hal-00771284

HAL Id: hal-00771284

<https://hal.science/hal-00771284v1>

Submitted on 8 Jan 2013

HAL is a multi-disciplinary open access archive for the deposit and dissemination of scientific research documents, whether they are published or not. The documents may come from teaching and research institutions in France or abroad, or from public or private research centers.

L'archive ouverte pluridisciplinaire **HAL**, est destinée au dépôt et à la diffusion de documents scientifiques de niveau recherche, publiés ou non, émanant des établissements d'enseignement et de recherche français ou étrangers, des laboratoires publics ou privés.

Phase diagram of the Anderson transition with atomic matter waves

M. Lopez¹, J.-F. Clément¹, G. Lemarié^{2,3}, D. Delande³,
P. Szriftgiser¹, J. C. Garreau^{1,4}

¹Laboratoire de Physique des Lasers, Atomes et Molécules, Université Lille 1 Sciences et Technologies, CNRS; F-59655 Villeneuve d'Ascq Cedex, France

²Laboratoire de Physique Théorique UMR-5152, CNRS and Université de Toulouse, F-31062 France

³Laboratoire Kastler-Brossel, UPMC-Paris 6, ENS, CNRS; 4 Place Jussieu, F-75005 Paris, France

⁴Corresponding author

E-mail: jean-claude.garreau@univ-lille1.fr

Abstract. We realize experimentally a cold atom system equivalent to the 3D Anderson model of disordered solids where the anisotropy can be controlled by adjusting an experimentally accessible parameter. This allows us to study experimentally the disorder vs anisotropy phase diagram of the Anderson metal-insulator transition. Numerical and experimental data compare very well with each other and a theoretical analysis based on the self-consistent theory of localization correctly describes the observed behavior, illustrating the flexibility of cold atom experiments for the study of transport phenomena in complex quantum systems.

PACS numbers: 03.75.-b , 64.70.Tg , 72.15.Rn

1. Introduction

The interplay of disorder and quantum interference has been an important subject in physics for more than 50 years. Quantum interferences, which are at the heart of most quantum effects, rely on precise relative phases between quantum trajectories, which are strongly sensitive to perturbations like decoherence (i.e. coupling with a large environment) and scattering of the wave function in potential wells. This last effect becomes particularly difficult to describe theoretically in a disordered system, in which these scattering processes have a random character. Intuitively, one easily understands that such kind of effect shall play an important role for example in the low-temperature electric conductance of solids. In fact, Anderson showed in 1958 that the presence of disorder might produce a *spatial localization* of the wavefunction, which *suppresses* conductivity [1] thus the name of “strong” localization.

Laser cooling opened the possibility of realizing very clean experiments in disordered systems, which generated a burst of interest on the subject. In adequate conditions, ultracold atoms placed in spatially structured laser beams feel this radiation as a mechanical potential acting on the center of mass variables of the atoms. Disordered potentials created in such a way allowed the realization of spatially disordered systems in one dimension [2, 3] and three dimensions [4, 5]. Despite these progresses, the Anderson metal-insulator transition (which manifests itself in 3 or more dimensions) is still very difficult to study in such systems, because Anderson localization requires a very strong disorder and – the cold atomic samples being prepared in the absence of disorder – the energy distribution of the atoms unavoidably spreads across the so-called *mobility edge*, an energy threshold separating localized and extended eigenstates. This in turn implies that the localized fraction, which can be *directly* measured in cold-atom experiments from the temporal evolution of the spatial probability distributions, remains small. Fortunately, one can find other systems also described by the Anderson localization physics, which are not a direct transposition of the condensed matter system, but rely on the profound analogy between quantum chaotic systems and disordered systems [6]. Using the quasiperiodic kicked rotor (QpKR) [7], an effectively 3D variant of the paradigmatic system of quantum chaos [8], the Anderson transition has been observed, its critical exponent measured experimentally [9, 10], its critical wavefunction characterized [11], and its class of universality firmly established [12], making this system an almost ideal environment to study Anderson type quantum phase transitions.

One advantage of this cold atom chaotic system as compared to other disordered systems is that the disorder can be controlled very precisely: the mean free path and the anisotropy are two experimentally tunable parameters. This allows us to present in this work an experimental study of the disorder vs anisotropy phase diagram of the Anderson transition, as well as an analytical description of these properties based on the self-consistent theory of Anderson localization, which brings another important brick to our detailed knowledge on the Anderson metal-insulator transition.

2. Controlled disorder and anisotropy within a cold atom system

The quasiperiodic kicked rotor is described by the one-dimensional time dependent Hamiltonian

$$H_{\text{qpkR}} = \frac{p^2}{2} + K \cos x (1 + \varepsilon \cos \omega_2 t \cos \omega_3 t) \sum_n \delta(t - n). \quad (1)$$

Experimentally, it is realized by placing laser-cooled atoms (of mass M) in a standing wave (formed by counterpropagating beams of intensity I_0 and wavenumber k_L) which generates an effective sinusoidal mechanical potential – nicknamed “optical potential” – $-\cos x$ acting on the center of mass position x of the atom. The standing wave is modulated by an acousto-optical modulator in order to form a periodic (of period T_1) train of short square pulses whose duration τ is short enough that, at the time scale of atom center of mass dynamics, they can be assimilated to Dirac δ - functions. The amplitude of such pulses is further modulated with frequencies ω_2 and ω_3 , proportionally to $1 + \varepsilon \cos \omega_2 t \cos \omega_3 t$. Lengths are measured in units of $(2k_L)^{-1}$, time in units of T_1 , momenta in units of $M/2k_L T_1$; note that $[x, p] = i\bar{k}$ with $\bar{k} = 4\hbar k_L^2 T_1 / M$ playing the role of a reduced Planck constant. The pulse amplitude is $K = \bar{k} \tau \Omega^2 / 8\Delta_L$, where Ω is the resonance Rabi frequency between the atom and the laser light and Δ_L the laser-atom detuning. Fixed parameters used throughout the present work are $\bar{k} = 2.885$, $\omega_2 = 2\pi\sqrt{5}$, $\omega_3 = 2\pi\sqrt{13}$ ‡.

If $\varepsilon = 0$ one obtains the standard kicked rotor, which is known to display fully chaotic classical dynamics for $K \geq 6$ [16]. At long time, the dynamics is a so-called chaotic diffusion in momentum space, which is – although perfectly deterministic – characterized by a diffusive increase of the r.m.s. momentum: $\langle p(t) - p(t=0) \rangle = 0$, $\langle [p(t) - p(0)]^2 \rangle \sim 2Dt$ (which D the classical diffusion constant) where the average $\langle \rangle$ is performed over an ensemble of trajectories associated with neighbouring initial conditions. The statistical distribution of $p(t)$ has the characteristic Gaussian shape of a diffusion process, whose width increases like \sqrt{t} . Quantum mechanically, this system displays the phenomenon of *dynamical localization*, that is, an asymptotic saturation of the average square momentum $\langle p^2 \rangle$ [8] at long time, that is localization in momentum space instead of chaotic diffusion, which has been proved to be a direct analog of the Anderson localization in one dimension [17, 18, 19].

If $2\pi/T_1, \omega_2, \omega_3, \bar{k}$ are incommensurable and $\varepsilon \neq 0$ one obtains the QpKR, which can be proven to be equivalent to the Anderson model in 3 dimensions [7, 10, 20, 21]. In a nutshell, the QpKR which is a 1-dimensional system with a time-dependent Hamiltonian depending on 3 different quasi-periods, can be mapped on a kicked “pseudo”-rotor, a 3-dimensional system with a time periodic Hamiltonian. As shown in detail in [10], both

‡ Rational values of $\omega_2/2\pi, \omega_3/2\pi$ produce a periodically – instead of quasiperiodically – kicked rotor, with different long time behaviour [13, 14, 15]. We chose “maximally irrational ratios” to avoid this problem.

systems share the same temporal dynamics. The Hamiltonian of the pseudo-rotor is:

$$\mathcal{H} = \frac{p_1^2}{2} + \omega_2 p_2 + \omega_3 p_3 + K \cos x_1 [1 + \varepsilon \cos x_2 \cos x_3] \sum_n \delta(t - n), \quad (2)$$

with an initial condition taken as a planar source in momentum space (completely delocalized along the transverse directions p_2 and p_3). Note that the kinetic energy has a different dependence on the momentum in each direction: standard (quadratic) in direction 1, but linear in directions 2 and 3; hence, the name pseudo-rotor.

The Hamiltonian (2) is periodic in configuration space. It can thus be expanded in a discrete momentum basis composed of states $|\mathbf{p}\rangle = |\mathbf{p} = \mathbf{k}\mathbf{p}\rangle$, where the \mathbf{p}_i are integers \S . In this basis, the evolution operator over one temporal period writes as the product $U = JV$ of an on-site operator: $V(\mathbf{p}) = e^{-i\phi_{\mathbf{p}}}$ with phases $\phi_{\mathbf{p}} = \frac{\mathbf{k}\mathbf{p}_1^2}{2} + \omega_2\mathbf{p}_2 + \omega_3\mathbf{p}_3$ and of a hopping operator J such that:

$$\langle \mathbf{p}_f | J | \mathbf{p}_i \rangle = \int \frac{d\mathbf{x}}{(2\pi)^3} \exp \left[-i \frac{K \cos x_1 (1 + \varepsilon \cos x_2 \cos x_3)}{\mathbf{k}} \right] \exp [-i(\mathbf{p}_i - \mathbf{p}_f)\mathbf{x}]. \quad (3)$$

The phases $V(\mathbf{p})$ are different on each site of the momentum lattice, and, although perfectly deterministic, constitute a pseudo-random sequence completely analogous to the true random on-site energies of the Anderson model. This makes it possible to identify V as the disorder operator for the QpKR. The parameter K controls the hopping amplitudes, that is the transport properties in the absence of disorder. The larger K , the larger distance the system propagates in momentum space (with the operator J) before being scattered by the disorder operator V . As shown below, the associated mean free path in momentum space is of the order of K/\mathbf{k} . Rather counter-intuitively, the weak disorder limit then corresponds to the large K limit, that is strong pulses, while the strong disorder limit where Anderson localization is expected corresponds to small K . It should also be stressed that, for very small K , (very strong disorder), the system remains frozen close to its initial state, with a trivial on-site Anderson localization. This is not really surprising as the classical dynamics is then regular instead of chaotic and even the classical chaotic diffusion is suppressed.

In the following, we will concentrate on the role of the ε parameter, which drives the anisotropy between the transverse directions and the longitudinal direction, showing the analogy of (2) with a system of weakly coupled disordered chains as considered in [22].

With such a system, we experimentally observed and characterized the Anderson transition [9, 10], which manifests itself by the fact that the momentum distribution is

\S This implies periodic boundary conditions. In general – especially for an "unfolded" rotor for x_1 is a position in real space as realized in the experiment – one should use the Bloch theorem which guarantees the existence of states whose wavefunction take a phase factor after translation by 2π . This amounts at considering not integer \mathbf{p}_i values, but rather $\mathbf{p}_i = n_i + \beta_i$ with n_i an integer and β_i a fixed quantity called quasimomentum. All conclusions obtained in the simplest case $\beta_i = 0$ can be straightforwardly extended in the general case.

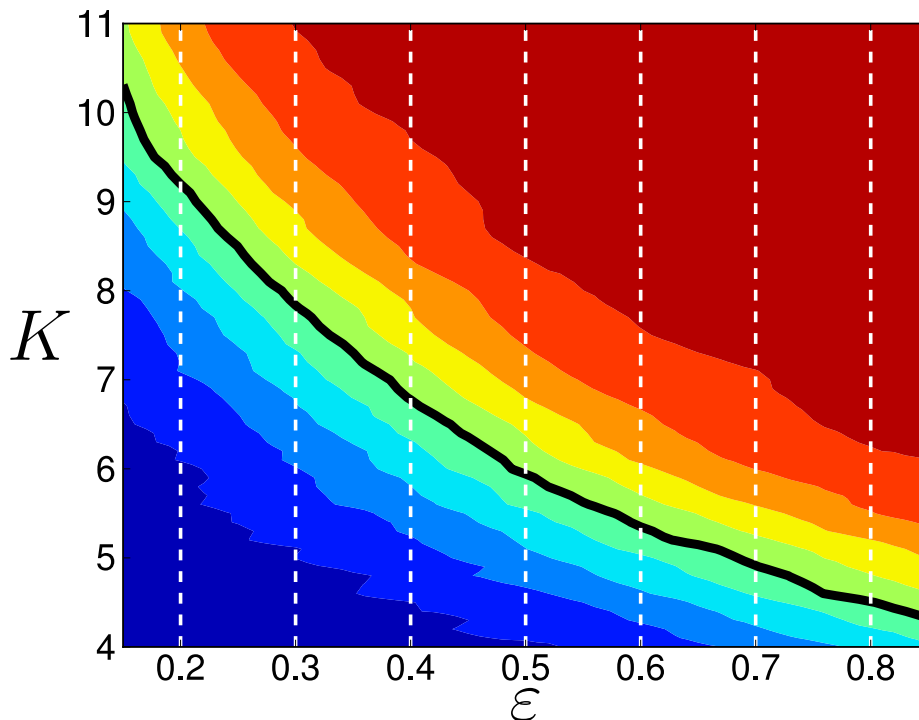


Figure 1. Schematic phase diagram of the metal-insulator Anderson transition for the quasi-periodic kicked rotor. The color plot corresponds to growth rate α of $\langle p^2(t) \rangle \propto t^\alpha$ at long time (1000 kicks for this plot), estimated from numerical simulations. Blue color represents localization ($\alpha = 0$), red represents diffusive dynamics ($\alpha = 1$). The black line corresponds to $\alpha = 2/3$, that is the critical line of the Anderson transition. Paths (white dashed lines) form the grid used for the determination of $K_c(\varepsilon)$.

exponentially localized $\Pi(\mathbf{p}; t) \sim \exp(-|\mathbf{p}|/\mathbf{p}_{\text{loc}})$ (with \mathbf{p}_{loc} the localization length) if K is smaller than a critical value $K_c(\varepsilon)$ and Gaussian diffusive $\Pi(\mathbf{p}; t) \sim \exp(-\mathbf{p}^2/4Dt)$ (where D is the diffusion coefficient) for $K > K_c(\varepsilon)$ after a sufficiently long time. At criticality, $K = K_c(\varepsilon)$, the localization length diverges, the diffusion constant vanishes, and the critical state is found [11] to have a characteristic Airy shape

$$\Pi(\mathbf{p}; t) \approx \frac{3}{2} \frac{\alpha}{\sqrt{\Lambda_c(\varepsilon)t^{2/3}}} \text{Ai} \left[\alpha \sqrt{\frac{|\mathbf{p}|^2}{\Lambda_c(\varepsilon)t^{2/3}}} \right] \quad (4)$$

following the anomalous diffusion at criticality: $\langle \mathbf{p}^2 \rangle = \Lambda_c(\varepsilon)t^{2/3}$ (here $\alpha = 3^{1/6}\Gamma(2/3)^{-1/2}$). The fundamental quantities characterizing the threshold of the transition are therefore $K_c(\varepsilon)$ and $\Lambda_c(\varepsilon)$, and we will consider in the following their dependence as a function of the anisotropy parameter ε .

3. Experimental determination of the anisotropy phase diagram

In our experience, we measure the population of the zero velocity class $\Pi(0; t)$ using Raman velocimetry [24, 25, 26]. This quantity is proportional to $\langle \mathbf{p}^2(t) \rangle$, with a

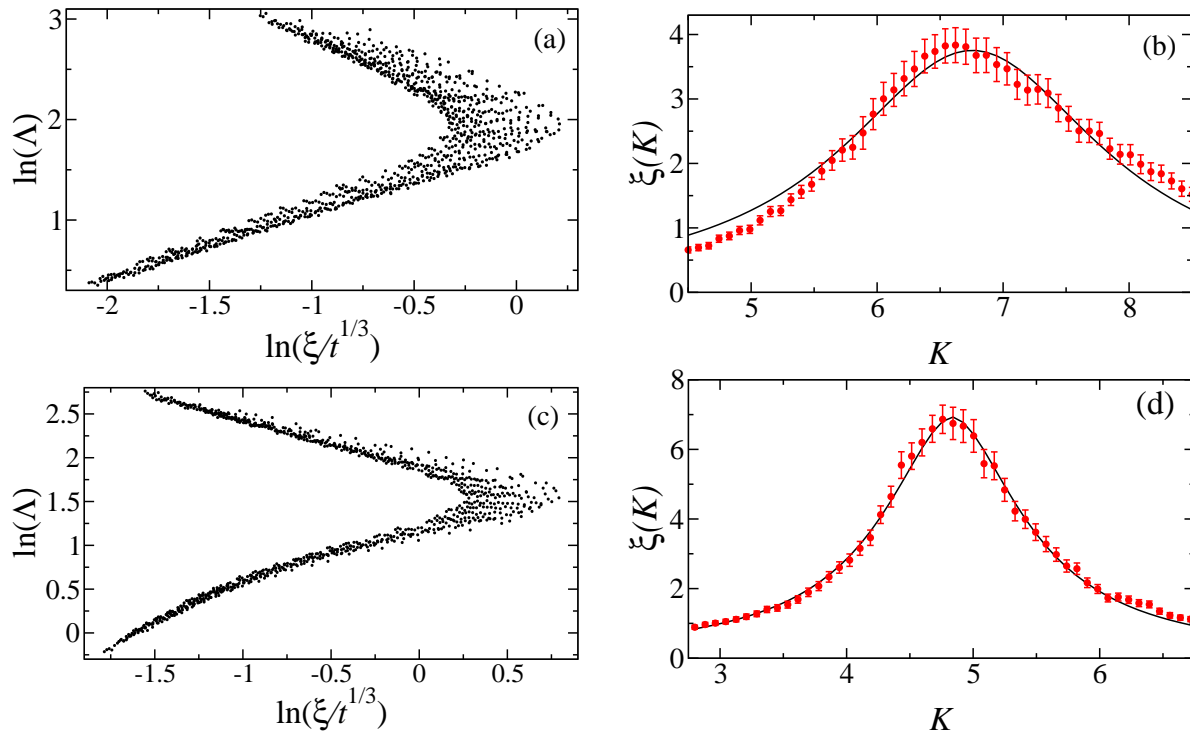


Figure 2. Determination of the critical point from experimental data at two different anisotropy ε . The finite-time scaling method (see text) applied to the experimental data $\Lambda(t) \propto \Pi(\mathbf{p} = 0; t)^{-2} t^{-2/3}$ allows for a determination of the scaling function F (Eq. (6)) represented in a and c and the scaling parameter $\xi(K)$ shown in b and d. The critical point corresponds to the tip at the right of the scaling function (see a and c), at the intersection of the diffusive (top) and localized branch (bottom). The marked maximum of $\xi(K)$ gives a precise determination of K_c . The parameters are: $\varepsilon = 0.4$ for a and b; $\varepsilon = 0.8$ for c and d. t varies up to 120 kicks.

ε	$K_1 - K_2$	K_c (exp)	K_c (num)	$\ln \Lambda_c$ (exp)	$\ln \Lambda_c$ (num)
0.2	7.0-14.0	8.85 ± 0.1	8.84 ± 0.47	2.1 ± 0.1	2.71 ± 0.44
0.3	5.2-9.2	7.46 ± 0.05	7.71 ± 0.42	2.05 ± 0.08	2.22 ± 0.34
0.4	4.5-8.5	6.75 ± 0.04	6.77 ± 0.52	1.95 ± 0.05	1.81 ± 0.47
0.5	4.0-8.0	6.00 ± 0.04	5.93 ± 0.37	1.85 ± 0.05	1.36 ± 0.46
0.6	3.4-7.4	5.59 ± 0.04	5.27 ± 0.35	1.75 ± 0.05	1.10 ± 0.30
0.7	2.9-6.9	5.27 ± 0.03	4.99 ± 0.34	1.60 ± 0.05	0.94 ± 0.40
0.8	2.8-6.8	4.84 ± 0.03	4.70 ± 0.43	1.52 ± 0.04	0.98 ± 0.31

Table 1. Experimental results on the determination of the critical point of the metal-insulator Anderson transition, for various values of the parameter ε of the quasi-periodic kicked rotor. The second column indicates the range of K where data has been taken. The experimentally measured values of both K_c and Λ_c are compared to the numerically calculated values. The uncertainties on the experimental data are rather small. The numerical data (with times up to 1000 kicks) have similar uncertainties, but also incorporate *systematic* shifts of (K_c, Λ_c) as a function of time [23] which cannot be estimated in the experimental data due to the restricted range of observation times $t \leq 120$ kicks.

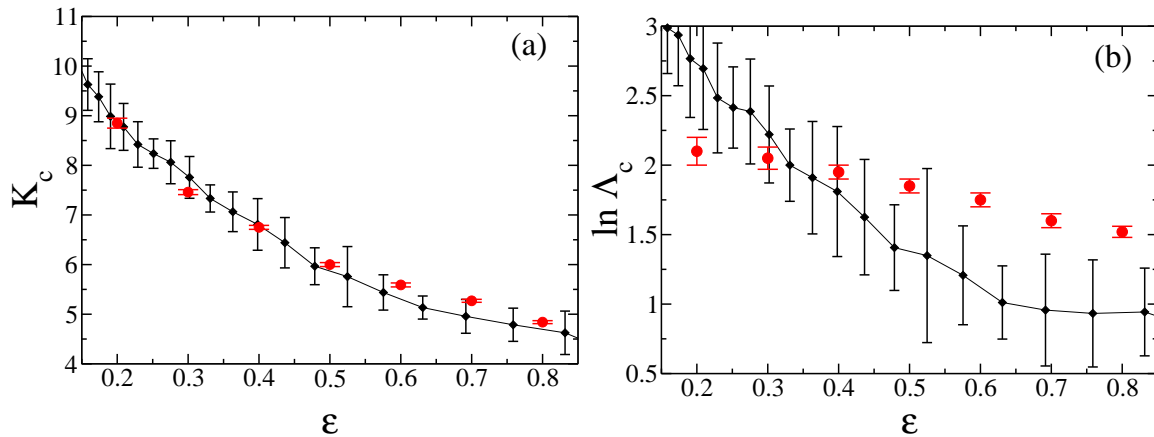


Figure 3. (a) Position of the critical point $K_c(\varepsilon)$, and (b) value of the critical $\Lambda_c(\varepsilon)$. Numerical results (black diamonds) and experimental measurements (red circles) are represented with their associated error bars. The uncertainties on the experimental data are rather small, as can be directly seen in fig. 2. The numerical data (with times up to 1000 kicks) have similar uncertainties, but also incorporate systematic deviations of (K_c, Λ_c) when estimated over various temporal ranges. These systematic deviations cannot be easily measured in the experiment (limited to 120 kicks). In plot (a) one observes a very good agreement between numerical and experimental results. The agreement is good in plot (b), except in the region of low ε where decoherence is expected to have a significant impact on the results and in the region of large ε where the finite variance of the initial momentum distribution tends to increase Λ_c at 120 kicks but has only small effect on K_c .

proportionality factor which depends on the specific shape of $\Pi(\mathbf{p})$. This factor varies smoothly across the Anderson transition, so that the transition can be studied using either $\langle \mathbf{p}^2(t) \rangle$ or $\Pi(0; t)$. The scaling theory of localization [27, 10] predicts that $\langle \mathbf{p}^2 \rangle$ has characteristic asymptotic behaviors in t^α , with $\alpha = 0$ in the localized regime, $\alpha = 2/3$ in the critical regime, and $\alpha = 1$ in the diffusive regime. This prediction has been fully confirmed by the experimental observations [11]. One can then define the *scaling variable* [9, 10]:

$$\Lambda(t) \equiv \frac{\langle \mathbf{p}^2(t) \rangle}{t^{2/3}} \propto \frac{1}{\Pi(\mathbf{p} = 0; t)^2 t^{2/3}}. \quad (5)$$

Asymptotically, $\Lambda(t) \propto t^{-2/3}, t^0, t^{1/3}$ in the localized, critical and diffusive regimes, respectively, so that $\ln \Lambda(t)$ vs $\ln t^{1/3}$ displays a positive slope 1 in the diffusive regime, zero slope at the critical point and negative slope -2 in the localized regime, which allows one to unambiguously identify the critical point. However, experimental limitations prevent us from performing measurements at large enough times (in our experiments typically $t_{\max} = 120$) to distinguish precisely between the localized and diffusive behaviors in the vicinity of the transition \parallel . The main causes of this limitation is the falling (under gravity action) of the cold atoms out of the standing wave and decoherence

\parallel Note however that for the parameters used here, $t_{\max}/t_{\text{loc}} \sim 10$ where t_{loc} is the localization time for the lowest K value used in each series at fixed ε , so that the lowest point is clearly in the localized regime.

induced by spontaneous emission.

Fortunately, a technique known as *finite size scaling* (which is finite *time* scaling in our case), based on arguments derived from the so-called *one parameter scaling theory* of the Anderson transition [27] allows us to overcome this limitation. The application of this technique to our problem has been discussed in details in previous works [10, 20, 28]; let us just say here that it relies on the verified hypothesis that Λ can be written as a one-parameter scaling function:

$$\Lambda = F \left(\frac{\xi(K)}{t^{1/3}} \right), \quad (6)$$

with the scaling parameter $\xi(K)$ which plays the role of the localization length p_{loc} in the localized regime and of the inverse of the diffusive constant in the diffusive regime. This method produces a rather precise determination of the critical parameters $K_c(\varepsilon)$ and $\Lambda_c(\varepsilon)$ and of the critical exponent of the Anderson transition [12] even from experimental signals limited to a hundred of kicks or so. An example of such a determination is presented in Fig. 2. The critical point corresponds to the tip at the right of the curve in Fig. 2a and c, at the intersection of the two clearly defined branches: A diffusive (top) and a localized branch (bottom). By construction, in principle $\xi(K)$ should diverge at the critical point, but the finite duration of the experiment and decoherence effects produce a cutoff; however, it still presents, as shown in Fig. 2b and d a marked maximum at the transition, and a careful fitting procedure taking these effects into account [12] allows a precise determination of K_c . Once the value of K_c has been determined according to the above technique, we measure the full momentum distribution, which is found to be in excellent agreement with the predicted Airy shape, eq. (4), as shown in [11]. A simple fit of the experimental data by an Airy function allows to measure $\langle \mathbf{p}^2 \rangle$, hence Λ_c .

We have measured the value of the critical parameters $K_c(\varepsilon)$ and $\Lambda_c(\varepsilon)$ [Eq. (5)] for a grid of 7 paths at constant ε in the parameter plane (K, ε) (see Fig. 1) For each path, 50 uniformly spaced values of K are used and the values of $\Pi(0; t)$ measured for each K value; the initial and final values of K are chosen symmetrically with respect to the critical point. For each value of K , an average of 20 independent measurements is performed, a full path thus corresponds to more than seven hours of data acquisition. Table 1 gives the details of each path and the results obtained.

Figure 3 displays the experimental and numerical results. Plot (a) indicates the position of the critical point $K_c(\varepsilon)$ and plot (b) the critical value $\Lambda_c(\varepsilon)$. In both plots, experimental measurements are indicated by red circles, numerical simulation results by black diamonds and are represented along with their error bars. The uncertainty of the numerical data (see the following for a discussion of the numerical method) is evaluated from data up to $t = 1000$ kicks and thus incorporates *systematic* shifts of (K_c, Λ_c) as a function of time [23] which cannot be estimated in the experimental data due to the restricted range of observation times $t \leq 120$ kicks. This results in larger numerical error bars than experimental ones. Note also that a small uncertainty in K_c

implies a much larger error in Λ_c due to its rapid variation as a function of K . In plot (a), one observes a very good agreement between numerical and experimental results. In plot (b), the agreement is good, except in the region of low ε which corresponds to high values of K and are thus more sensitive to decoherence effects. In the region of large ε , the finite variance of the initial momentum distribution tends to increase the experimental Λ_c , an effect which is not present in the numerical data.

4. Self-consistent theory of the anisotropy phase diagram

We shall now try to describe theoretically the observed anisotropy dependences of the two critical parameters $K_c(\varepsilon)$ and $\Lambda_c(\varepsilon)$. The approach we shall follow is based on the self-consistent theory of localization [29] which has been used successfully to predict numerous properties of the Anderson transition, and in particular the disorder vs energy [30] and disorder vs anisotropy [22] phase diagrams of the 3D Anderson model. Moreover, the self-consistent theory of localization has been transposed to the case of the kicked rotor [31, 32]. We will use in the following a simple generalization of this latter approach adapted to the case of the 3D anisotropic kicked pseudo-rotor (2) corresponding to the quasiperiodic 1D kicked rotor.

The starting point is to consider the probability to go from a site \mathbf{p}_i to a site \mathbf{p}_f in N steps, $P(\mathbf{p}_i, \mathbf{p}_f, t = N) \equiv |\langle \mathbf{p}_f | U^N | \mathbf{p}_i \rangle|^2$. It consists in propagations mediated by the hopping amplitudes $\langle \mathbf{p}_{n+1} | J | \mathbf{p}_n \rangle$ and by collisions on the disorder represented by $V(\mathbf{p}) = e^{-i\phi_{\mathbf{p}}}$. Two important points are the following: (i) one can consider in a first approximation the $\phi_{\mathbf{p}}$ as completely random phases [17, 33, 34] and we will consider quantities averaged over those phases, for example $\overline{P}(\mathbf{p}_i, \mathbf{p}_f, t = N)$ where the line over the quantity represents this averaging; (ii) $\langle \mathbf{p}_{n+1} | J | \mathbf{p}_n \rangle$ plays the role of the disorder averaged Green's function (in the usual language of diagrammatic theory of transport in disordered systems [35]), that is the propagation between two scattering events. Indeed, when $\varepsilon = 0$ and in the direction p_1 , this is just a Bessel function which decreases exponentially fast for $|\mathbf{p}_{n+1} - \mathbf{p}_n| \gg K/\bar{k}$ and one can thus see K/\bar{k} as the analog of the mean free path, with the limit of small disorder corresponding to $K/\bar{k} \gg 1$.

One can attack the problem of the calculation of \overline{P} by looking for propagation terms – including of course interference patterns – which survive the disorder averaging. At lowest order, the contribution containing no interference term to the probability \overline{P} is called the Diffuson [35]. It corresponds to the classical chaotic diffusion and can be shown to have a diffusive kernel expressed in the reciprocal space (\mathbf{q}, ω) (conjugated to (\mathbf{p}, t)) as [31, 32, 20]:

$$\overline{P}_D(\mathbf{q}, \omega) = \frac{1}{-i\omega + \sum_j D_{jj} q_j^2}. \quad (7)$$

Here, the diffusive tensor \mathbf{D} – computed in [36] for large K – is anisotropic, but diagonal,

with:

$$\begin{aligned} D_{11} &= \frac{K^2}{4k^2} \left(1 + \frac{\varepsilon^2}{4} \right), \\ D_{22} = D_{33} &= \frac{K^2 \varepsilon^2}{16k^2}. \end{aligned} \quad (8)$$

This anisotropic diffusive kernel is valid at long times and on large scale in momentum space, that is in the so-called hydrodynamic limit $\omega \ll 1$ and $q_j k_j \ll 1$, with k_j the mean free path along direction j which is such that $D_{jj} = k_j^2/4$. Equation (7) means that in the regime of long times and large distances (in momentum space), we should have a diffusive transport with $\langle \mathbf{p}_j^2 \rangle = 2D_{jj}t$. This is certainly not the case near the Anderson transition, which implies that we must go beyond the Diffuson approximation.

The simplest interferential correction – known as weak localization correction – is due to the constructive interference between pairs of time-reversed paths ¶, or equivalently to the maximally crossed diagrams, or Cooperon. The net effect of these interferential contributions is to increase the return probability at the initial point and to decrease the diffusion constant. It is possible to compute perturbatively the weak localization correction as an integral (see below) depending on the diffusion constant itself. Contributions from higher orders are extremely complicated and there is no systematic way of summing them all.

The self-consistent theory of localization is a simple attempt at approximately summing the most important contributions: instead of computing the weak localization correction using the raw diffusion constant, one uses the one renormalized because of weak localization. The whole thing must of course be self-consistent, so that the diffusion constant computed taking into account the weak localization correction is equal to the one input in the calculation of this correction. The price to pay is that one can no longer define a single diffusion constant – or, in the anisotropic case, a single diffusion tensor – but must introduce a frequency-dependent diffusion constant (or diffusion tensor). This is nevertheless quite natural if one wants to describe the transition from a diffusive behaviour as short time (large frequency) when interference terms are small to a localized behaviour at long time (small frequency). The intensity propagator \bar{P} takes then the approximate form: $\bar{P}(\mathbf{q}, \omega) = \frac{1}{-i\omega + \sum_j \mathcal{D}_{jj}(\omega) q_j^2}$ with the frequency dependent diffusion constant following the self-consistent equation [20, 29, 31]:

$$\mathcal{D}_{ii}(\omega) = D_{ii} - 2\mathcal{D}_{ii}(\omega) \int \frac{d^3\mathbf{q}}{(2\pi)^3} \frac{1}{-i\omega + \sum_j \mathcal{D}_{jj}(\omega) q_j^2}. \quad (9)$$

Quite remarkably, this approach is able to account for a certain number of observed features: it predicts a transition between a metallic phase of diffusive transport for $K > K_c(\varepsilon)$ where $\mathcal{D}_{ii}(\omega) \underset{\omega \rightarrow 0}{\sim} \mathcal{D}_{ii}(0) > 0$, to a localized phase for $K < K_c(\varepsilon)$ where $\mathcal{D}_{ii}(\omega) \underset{\omega \rightarrow 0}{\sim} -i\omega \mathbf{p}_{\text{loc}i}^2$ with $\mathbf{p}_{\text{loc}i}$ the localization length along direction i . At the threshold,

¶ The quasi-periodic kicked rotor or the equivalent periodic 3D pseudo-rotor is not invariant by time reversal. However, the Hamiltonian, eq. (2), is invariant by the product of time reversal and parity. The existence of such an anti-unitary symmetry is sufficient for the system to belong to the Orthogonal universality class, and consequently for the existence of the weak localization correction.

the transport is predicted to follow an anomalous diffusion with $\mathcal{D}_{ii}(\omega) \sim (-i\omega)^{1/3}$ and this implies the Airy shape of the critical state observed experimentally [11]. In the following, we will calculate explicitly the critical parameters $K_c(\varepsilon)$ and $\Lambda_c(\varepsilon)$ from (9) and show that it also complies well with the experimental observations.

One shall evaluate the integral on the right hand side of equation (9). It is important to remark that, although the system is anisotropic and thus 3 different equations (9) have to be solved simultaneously, they in fact follow exactly the same renormalization scheme: dividing eq. (9) by D_{ii} produces the same equation in all 3 dimensions. In other words, there is no anomaly in the anisotropic character at the critical point.

It is well known [29] that in dimension $d \geq 2$, the results of the self-consistent theory are cutoff dependent. Indeed, the integral in (9) diverges at large q and must be limited to $q_j < q_j^{\max}$, where q_j^{\max} is a cutoff on the order of k_j^{-1} , i.e. the inverse of the mean free path. In the following, we will take [22] $q_j^{\max} \equiv C_1 k_j^{-1} = C_1 / (2\sqrt{D_{jj}})$ with C_1 a numerical constant of the order of one. We make the following change of variables: $Y_j = \sqrt{\frac{\mathcal{D}_{jj}(\omega)}{-i\omega}} q_j$ and define the rescaled cutoff: $\ell(\omega) \equiv \sqrt{\frac{\mathcal{D}_{jj}(\omega)}{-i\omega}} q_j^{\max}$ (from Eq. (9) it is clear that the ratio $\mathcal{D}_{jj}(\omega)/D_{jj}$ is isotropic, thus $\ell(\omega)$ is isotropic). One obtains:

$$\frac{\mathcal{D}_{ii}(\omega)}{D_{ii}} = 1 - \frac{C_1}{2\pi^2} \frac{1}{\sqrt{D_{11}D_{22}D_{33}}} \left[1 - \frac{\tan^{-1} \ell(\omega)}{\ell(\omega)} \right]. \quad (10)$$

The threshold $K_c(\varepsilon)$ of the Anderson transition is then approached from the diffusive regime, which is characterized by $\frac{\mathcal{D}_{ii}(\omega)}{D_{ii}} \xrightarrow{\omega \rightarrow 0} \frac{\mathcal{D}_{ii}(0)}{D_{ii}} \xrightarrow{K \rightarrow K_c} 0$ and $\ell(\omega) \xrightarrow{\omega \rightarrow 0} \infty$. Therefore, $K_c(\varepsilon)$ is such that:

$$D_{11}D_{22}D_{33} = \frac{C_1^2}{4\pi^4}. \quad (11)$$

From the above expressions (8) for the diffusion tensor, one deduces the following dependence of the threshold vs anisotropy:

$$K_c(\varepsilon) = \left(\frac{2^4 C_1}{\pi^2} \right)^{1/3} \frac{k}{(\varepsilon^2 \sqrt{1 + \varepsilon^2/4})^{1/3}}. \quad (12)$$

The self-consistent theory allows also for a determination of $\Lambda_c(\varepsilon)$. In fact, at finite but sufficiently small ω (i.e. at sufficiently large times), $\ell(\omega)$ is large and one can evaluate the right hand side of (10) at the lowest order in $1/\ell(\omega)$ which gives:

$$\frac{\mathcal{D}_{ii}(\omega)}{(-i\omega)^{1/3}} = \frac{1}{(2\pi)^{2/3}} \frac{D_{11}}{(D_{11}D_{22}D_{33})^{1/3}}. \quad (13)$$

We know from the study of the critical state of the Anderson transition [11] that $\frac{\mathcal{D}_{11}(\omega)}{(-i\omega)^{1/3}} = \frac{\Gamma(2/3)}{3} \Lambda_c$ which allows us to write:

$$\Lambda_c(\varepsilon) = \frac{3}{\Gamma(2/3)} \left(\frac{1}{2\pi} \right)^{2/3} \left(\frac{D_{11}^2}{D_{22}D_{33}} \right)^{1/3}. \quad (14)$$

Using the diffusion tensor relations (8), one obtains finally:

$$\Lambda_c(\varepsilon) = \frac{3}{\Gamma(2/3)} \left(\frac{2}{\pi}\right)^{2/3} \left(\frac{1 + \varepsilon^2/4}{\varepsilon^2}\right)^{2/3}. \quad (15)$$

Equations (12) and (15) are the most important results of this section. They predict that the threshold $K_c(\varepsilon)$ and the critical anomalous diffusion parameter $\Lambda_c(\varepsilon)$ diverge at large anisotropy as $K_c(\varepsilon) \sim \varepsilon^{-2/3}$ and $\Lambda_c(\varepsilon) \sim \varepsilon^{-4/3}$. Therefore, when $\varepsilon = 0$ we recover the case of the 1D periodic kicked rotor which is always localized whatever the kicking amplitude K .

5. Experimental and numerical tests of the self-consistent theory of the anisotropy phase diagram

In order to test the predictions of the self-consistent theory, we have performed numerical simulations of the dynamics of the quasi-periodic kicked rotor (1). We have determined the critical parameters $K_c(\varepsilon)$ and $\Lambda_c(\varepsilon)$ from the crossing of the curves $\ln \Lambda = \ln \frac{\langle \mathbf{p}^2 \rangle}{t^{2/3}}$ vs K at different times (see figure 4). At the critical point, $\Lambda(t)$ is a constant $\Lambda(t) = \Lambda_c(\varepsilon)$ corresponding to the critical anomalous diffusion $\langle \mathbf{p}^2 \rangle \sim t^{2/3}$ and the crossing of the curves in fig. 4, whereas for $K < K_c(\varepsilon)$ ($K > K_c(\varepsilon)$, resp.), $\Lambda(t)$ decreases (increases, resp.) as time increases. We have evaluated the uncertainty of the parameters (K_c, Λ_c) by the region where the evolution of $\Lambda(t)$ is not monotonous (due to systematic shifts of (K_c, Λ_c) as a function of time [23]). The results are represented in fig. 5 for $K_c(\varepsilon)$ and in fig. 6 for $\Lambda_c(\varepsilon)$ by the white filled region between the blue filled region where the system is localized and pink filled region where the dynamics is diffusive. The data seem to follow an algebraic increase as the anisotropy parameter ε decreases (linear dependence in log-log scale as in figs. 5 and 6), on top of which oscillations are also clearly seen.

The self-consistent theory discussed in the previous section predicts that the critical regime of the Anderson transition is given by Eq. (11). Various approximations – leading to slightly different predictions for the position of the critical point – can be used for the values of the components of the diffusion tensor:

- (i) The simplest approximation is to use eq. (8), valid asymptotically for large K . This results in the simple analytic predictions (12) and (15), represented by black lines in figures 5 and 6. The algebraic dependences of $K_c(\varepsilon)$ and $\Lambda_c(\varepsilon)$ are well accounted for by these simple predictions, however they fail to reproduce the oscillating corrections observed in the numerical data.
- (ii) The theoretical prediction (8) for the diffusion tensor \mathbf{D} miss the oscillations of the diffusion tensor of the 3D kicked pseudo-rotor (2) vs K and \hbar . Such oscillations are well known in the case of the 1D periodic kicked rotor [37, 33] and arise due to subtle temporal correlation effects. In our case, we have checked that they could be described approximately by the known oscillating form [33], but only along direction

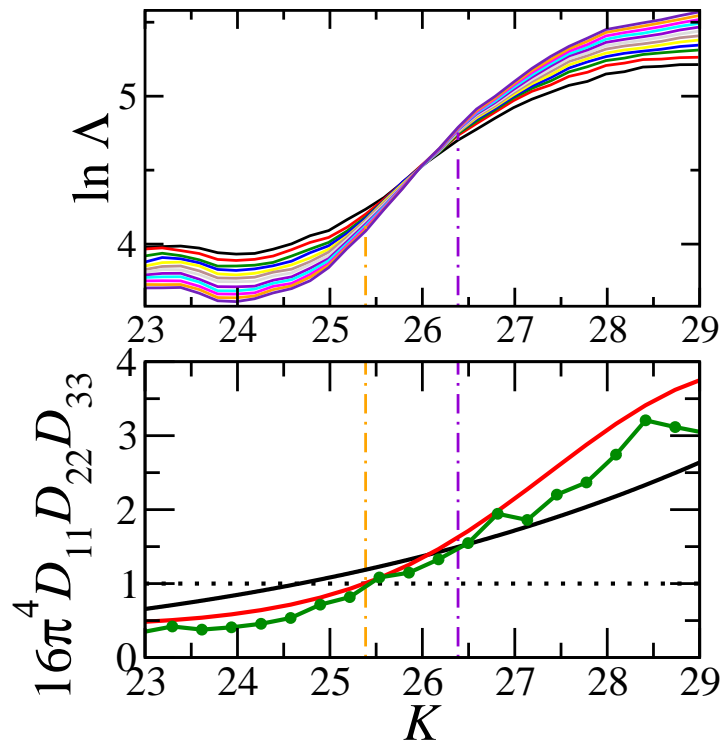


Figure 4. Method of determination of the threshold $K_c(\varepsilon)$. Upper panel: Numerical data for $\ln \Lambda = \ln \frac{\langle \mathbf{p}^2 \rangle}{t^{2/3}}$ vs K at different times ranging from $t = 36$ to 956 . The threshold corresponds to the crossing of these lines where we have the critical anomalous diffusion $\langle \mathbf{p}^2 \rangle \sim t^{2/3}$, whereas for $K < K_c(\varepsilon)$, $\Lambda(t)$ decreases at long time (localized regime) and for $K > K_c(\varepsilon)$ $\Lambda(t)$ increases at long time (metallic regime). The uncertainty region (between the orange and violet dash-dotted lines) corresponds to the region where the evolution of $\Lambda(t)$ is not monotonous. Lower panel: The different degrees of approximation for $16\pi^4 D_{11} D_{22} D_{33}$. According to Eq. (11) (with $C_1 = 1/2$, see text), this quantity should be equal to unity at the critical point. The black line corresponds to the simple analytic prediction (8) for the diffusion tensor. The red line shows the theoretical prediction incorporating oscillating corrections for the diffusion tensor (see Eq. (16) and text). The green line with points shows numerical data for the diffusion tensor \mathbf{D} of the 3D kicked rotor (2), at short time. The parameters are: $\tilde{k} = 2.89$, $\omega_2 = 2\pi\sqrt{5}$ and $\omega_3 = 2\pi\sqrt{13}$, $\varepsilon = 0.036$.

1:

$$\begin{aligned} \tilde{D}_{11} &\approx D_{11} \times \{1 - 2J_2(\tilde{K})[1 - J_2(\tilde{K})]\}, \\ \tilde{D}_{22} &= \tilde{D}_{33} = D_{22} = D_{33}. \end{aligned} \quad (16)$$

with $\tilde{K} \equiv K \frac{\sin \tilde{k}/2}{\tilde{k}/2}$ and J_2 the usual Bessel function. The use of the above equation for the diffusion tensor allows for a better analytical description of the anisotropy phase diagram, see the red lines in figures 5 and 6.

- (iii) The third type of approximation relies on a direct numerical calculation of the diffusion tensor \mathbf{D} of the 3D kicked rotor (2) at short time by a linear fitting procedure over the first ten kicks of $\langle \mathbf{p}_i^2 \rangle = 2D_{ii}t$. This gives a numerical prediction of the self-consistent theory for the anisotropy phase diagram represented by the

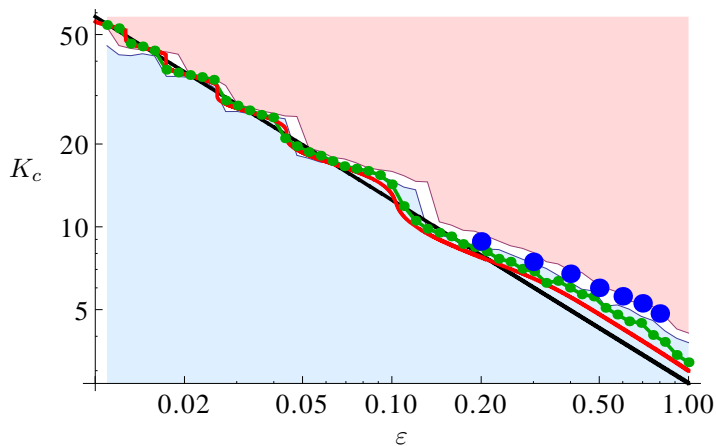


Figure 5. Threshold of the Anderson transition vs anisotropy (log-log scale). The anisotropy dependence of $K_c(\varepsilon)$ with the associated uncertainty is determined from numerical simulations of the dynamics of the quasi-periodic kicked rotor and is represented by the white filled region between the blue (localized) and pink (metallic) filled regions. The three degrees of approximation of the self-consistent theory prediction (11) (with $C_1 = 1/2$) are shown: (i) the black line corresponds to the simple analytic prediction (12), (ii) the red line incorporates oscillating corrections for the diffusion tensor (see Eq. (16) and text) while (iii) the green line with points corresponds to numerical data for the diffusion tensor \mathbf{D} of the 3D kicked rotor (2), at short time. The blue points represent the experimental data. The parameters are: $\tilde{k} = 2.89$, $\omega_2 = 2\pi\sqrt{5}$ and $\omega_3 = 2\pi\sqrt{13}$.

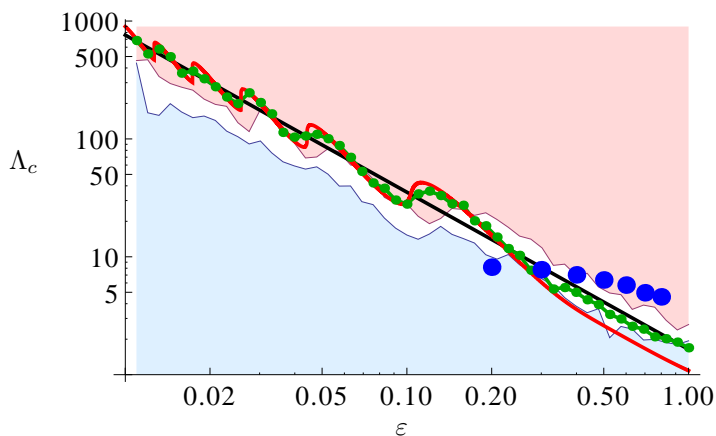


Figure 6. Critical parameter Λ_c vs anisotropy (log-log scale). The anisotropy dependence of $\Lambda_c(\varepsilon)$ with the associated uncertainty is determined from numerical simulations of the dynamics of the quasi-periodic kicked rotor and is represented by the white filled region between the blue (localized) and pink (metallic) filled regions. The prediction (14) of the self-consistent theory is shown with the three different degrees of approximations considered: (i) the simple analytic prediction (15) is shown in black line, (ii) the red lines is based on the analytic prediction Eq. (16) for the diffusion tensor incorporating oscillating corrections in K and \tilde{k} and (iii) numerical data for the diffusion tensor \mathbf{D} of the 3D kicked rotor at short time (2) give the green line with points. The blue points represent the experimental data. The parameters are: $\tilde{k} = 2.89$, $\omega_2 = 2\pi\sqrt{5}$ and $\omega_3 = 2\pi\sqrt{13}$.

green lines with points in figures 5 and 6. They clearly show oscillations around the power law behaviors of $K_c(\varepsilon)$ and $\Lambda_c(\varepsilon)$, and are in very good agreement with the numerical data.

Last but not least, we clearly see in fig. 5 and 6 that the predictions of the self-consistent theory agree also very well with the experimental data represented by blue points. Therefore, the self-consistent theory appears to be a powerful way to describe the Anderson transition with the quasi-periodic kicked rotor.

6. Conclusion

In conclusion, we presented in this work a rather complete study of the anisotropy phase diagram of the Anderson transition in the quasiperiodic kicked rotor. Numerical and experimental results were found to be in good agreement with each other, and theoretical expressions based on the self-consistent theory of the Anderson transition correctly describe the shape dependence of these functions. These results bring an important additional brick to our understanding of the Anderson transition, and put in an even firmer ground the status of the quasiperiodic kicked rotor as one of the simplest – if not the simplest – cold atom system for experimentally studying Anderson localization.

Acknowledgments

Laboratoire de Physique des Lasers, Atomes et Molécules is Unité Mixte de Recherche 8523 of CNRS. Work partially supported by Agence Nationale de la Recherche (LAKRIDI grant) and “Labex” CEMPI. CPU time on various computers has been provided by GENCI.

References

- [1] P. W. Anderson. Absence of Diffusion in Certain Random Lattices. *Phys. Rev.*, 109(5):1492–1505, 1958.
- [2] J. Billy, V. Josse, Z. Zuo, A. Bernard, B. Hambrecht, P. Lugan, D. Clément, L. Sanchez-Palencia, P. Bouyer, and A. Aspect. Direct observation of Anderson localization of matter-waves in a controlled disorder. *Nature (London)*, 453:891–894, 2008.
- [3] G. Roati, C. d’Errico, L. Fallani, M. Fattori, C. Fort, M. Zaccanti, G. Modugno, M. Modugno, and M. Inguscio. Anderson localization of a non-interacting Bose-Einstein condensate. *Nature (London)*, 453:895–898, 2008.
- [4] S. S. Kondov, W. R. McGehee, J. J. Zirbel, and B. DeMarco. Three-Dimensional Anderson Localization of Ultracold Matter. *Science*, 334(6052):66–68, 2011.
- [5] F. Jendrzejewski, A. Bernard, K. Mueller, P. Cheinet, V. Josse, M. Piraud, L. Pezzé, L. Sanchez-Palencia, A. Aspect, and P. Bouyer. Three-dimensional localization of ultracold atoms in an optical disordered potential. *Nature Physics*, 8:398, 2012.
- [6] K. Efetov. *Supersymmetry in Disorder and Chaos*. Cambridge University Press, Cambridge, UK, 1997.

- [7] G. Casati, I. Guarneri, and D. L. Shepelyansky. Anderson transition in a one-dimensional system with three incommensurable frequencies. *Phys. Rev. Lett.*, 62(4):345–348, 1989.
- [8] G. Casati, B. V. Chirikov, J. Ford, and F. M. Izrailev. *Stochastic behavior of a quantum pendulum under periodic perturbation*, volume 93, pages 334–352. Springer-Verlag, Berlin, Germany, 1979.
- [9] J. Chabé, G. Lemarié, B. Grémaud, D. Delande, P. Szriftgiser, and J. C. Garreau. Experimental Observation of the Anderson Metal-Insulator Transition with Atomic Matter Waves. *Phys. Rev. Lett.*, 101(25):255702, 2008.
- [10] G. Lemarié, J. Chabé, P. Szriftgiser, J. C. Garreau, B. Grémaud, and D. Delande. Observation of the Anderson metal-insulator transition with atomic matter waves: Theory and experiment. *Phys. Rev. A*, 80(4):043626, 2009.
- [11] G. Lemarié, H. Lignier, D. Delande, P. Szriftgiser, and J. C. Garreau. Critical State of the Anderson Transition: Between a Metal and an Insulator. *Phys. Rev. Lett.*, 105(9):090601, 2010.
- [12] M. Lopez, J.-F. Clément, P. Szriftgiser, J. C. Garreau, and D. Delande. Experimental Test of Universality of the Anderson Transition. *Phys. Rev. Lett.*, 108(9):095701, 2012.
- [13] J. Ringot, P. Szriftgiser, J. C. Garreau, and D. Delande. Experimental Evidence of Dynamical Localization and Delocalization in a Quasiperiodic Driven System. *Phys. Rev. Lett.*, 85(13):2741–2744, 2000.
- [14] H. Lignier, J. C. Garreau, P. Szriftgiser, and D. Delande. Quantum diffusion in the quasiperiodic kicked rotor. *EPL (Europhysics Letters)*, 69(3):327–333, 2005.
- [15] H. Lignier, J. Chabé, D. Delande, J. C. Garreau, and P. Szriftgiser. Reversible Destruction of Dynamical Localization. *Phys. Rev. Lett.*, 95(23):234101, 2005.
- [16] B. V. Chirikov. A universal instability of many-dimensional oscillator systems. *Phys. Rep.*, 52(5):263–379, 1979.
- [17] S. Fishman, D. R. Grempel, and R. E. Prange. Chaos, Quantum Recurrences, and Anderson Localization. *Phys. Rev. Lett.*, 49(8):509–512, 1982.
- [18] Alexander Altland and Martin R. Zirnbauer. Field theory of the quantum kicked rotor. *Phys. Rev. Lett.*, 77:4536–4539, Nov 1996.
- [19] Chushun Tian and Alexander Altland. Theory of localization and resonance phenomena in the quantum kicked rotor. *New Journal of Physics*, 12(4):043043, 2010.
- [20] G. Lemarié. *Transition d’Anderson avec des ondes de matière atomiques*. PhD thesis, Université Pierre et Marie Curie, Paris, 2009.
- [21] C. Tian, A. Altland, and M. Garst. Theory of the Anderson Transition in the Quasiperiodic Kicked Rotor. *Phys. Rev. Lett.*, 107(7):074101, 2011.
- [22] I. Zambetaki, Qiming Li, E. N. Economou, and C. M. Soukoulis. Localization in highly anisotropic systems. *Phys. Rev. Lett.*, 76:3614–3617, May 1996.
- [23] K. Slevin and T. Ohtsuki. Corrections to Scaling at the Anderson Transition. *Phys. Rev. Lett.*, 82(2):382–385, 1999.
- [24] J. Ringot, P. Szriftgiser, and J. C. Garreau. Subrecoil Raman spectroscopy of cold cesium atoms. *Phys. Rev. A*, 65(1):013403, 2001.
- [25] J. Chabé, H. Lignier, P. Szriftgiser, and J. C. Garreau. Improving Raman velocimetry of laser-cooled cesium atoms by spin-polarization. *Opt. Commun.*, 274:254–259, 2007.
- [26] J. Ringot, Y. Lecoq, J. Garreau, and P. Szriftgiser. Generation of phase-coherent laser beams for Raman spectroscopy and cooling by direct current modulation of a diode laser. *Eur. Phys. J. D*, 7(3):285–288, 1999.
- [27] E. Abrahams, P. W. Anderson, D. C. Licciardello, and T. V. Ramakrishnan. Scaling Theory of Localization: Absence of Quantum Diffusion in Two Dimensions. *Phys. Rev. Lett.*, 42(10):673–676, 1979.
- [28] G. Lemarié, B. Grémaud, and D. Delande. Universality of the Anderson transition with the quasiperiodic kicked rotor. *EPL (Europhysics Letters)*, 87:37007, 2009.
- [29] D. Vollhardt and P. Wölfle. Self-Consistent Theory of Anderson Localization. In Hanke, W. and Kopaev Yu. V., editor, *Electronic Phase Transitions*, pages 1–78. Elsevier, 1992.

- [30] J. Kroha, T. Kopp, and P. Wölfle. Self-consistent theory of anderson localization for the tight-binding model with site-diagonal disorder. *Phys. Rev. B*, 41:888–891, Jan 1990.
- [31] Alexander Altland. Diagrammatic approach to anderson localization in the quantum kicked rotator. *Phys. Rev. Lett.*, 71:69–72, Jul 1993.
- [32] C. Tian, A. Kamenev, and A. Larkin. Ehrenfest time in the weak dynamical localization. *Phys. Rev. B*, 72:045108, Jul 2005.
- [33] D. L. Shepelyansky. Localization of diffusive excitation in multi-level systems. *Physica D*, 28:103–114, 1987.
- [34] Meir Griniasty and Shmuel Fishman. Localization by pseudorandom potentials in one dimension. *Phys. Rev. Lett.*, 60:1334–1337, Mar 1988.
- [35] E. Akkermans and G. Montambaux. *Mesoscopic physics of electrons and photons*. Cambridge Univ Pr, 2007.
- [36] G. Lemarié, D. Delande, J. C. Garreau, and P. Szriftgiser. Classical diffusive dynamics for the quasiperiodic kicked rotor. *J. Mod. Opt.*, 57(19):1922–1927, 2010.
- [37] A. B. Rechester, M. N. Rosenbluth, and R. B. White. Fourier-space paths applied to the calculation of diffusion for the Chirikov-Taylor model. *Phys. Rev. A*, 23(5):2664–2672, 1981.